Self-Biased Low Loss Conductor Featured With Skin Effect Suppression for High Quality RF Passives

I. Iramnaaz[1], H. Schellevis[2], B. Rejaei[3], R. Fitch[4], and Y. Zhuang[1]

[1]Department of Electrical Engineering, Wright State University, Dayton, OH 45435 USA
[2]Department of Electrical Engineering, Delft University of Technology, Delft, The Netherlands
[3]Department of Electrical Engineering, Sharif University of Technology, Tehran, Iran
[4]Sensors Directorate, Air Force Research Laboratory, Wright-Patterson AFB, OH 45433 USA

We present experimental data for artificial metaconductors exhibiting skin effect suppression at microwave frequencies. The metaconductor consists of a stack comprising twelve periods of alternating ferromagnetic (Permalloy) and normal metal (Cu) layers. Near the effective antiferromagnetic resonant frequency the average in-plane magnetic permeability of the stack approaches zero, leading to an increase in the skin depth. Compared to a Cu-based device, up to 70% loss reduction has been achieved by a metaconductor based coplanar wave guide at ∼10 GHz without changing the propagation wavelength. Moreover, unlike conventional magnetic devices, no external magnetic bias is required due to the large magnetic anisotropy present in the ferromagnetic layers.

***Index Terms*—Coplanar wave guide, ferromagnetic resonance, magnetic thin film, metamaterial, radio frequency.**

I. Introduction

MONOLITHIC integration of high-speed giga-/tera- scale electronics is critically impeded by the so-called interconnect RC delay or latency [1]–[3] which imposes formidable limits on speed, energy dissipation and signal integrity [4]–[9]. In particular, synchronous clock distribution networks for high performance microprocessors rely on minimizing the interconnect latency to counter the degradation of clock-edge integrity and, consequently, to raise up the clock frequency [6]. Compared to the transistors, typical interconnects of the 35-nm generation show more than 100-times larger switching delay, and prevailing energy dissipation [8]. Further increase of the integration density of multigigahertz microprocessors into the terascale imposes even more severe challenges on interconnect loss and latency [5].

To reduce the interconnect RC delay, materials with a low relative dielectric constant are already widely adopted for reducing the interconnect–interconnect and interconnect-substrate capacitance [1], [10]. At its best, however, one can expect an additional ∼ 2-fold reduction of the latter even by use of an ideal medium (vacuum). Further improvement must thus come from an improved conductivity. At high frequencies, the ohmic loss in all naturally existing conductors is unexceptionally governed by its finite conductivity σ and the skin effect. The tendency for the electric current at high frequency to flow mostly near the surface of the conductor within the surface depth $\delta = \sqrt{1/\pi f \sigma \mu_0}$ is called skin effect, where f is the frequency of the signal and μ_0 is the vacuum permeability. Copper is the metal of choice in today's integrated electronics. Due to its high conductivity $(6 \times 10^7\ \mathrm{S/m})$, reducing ohmic loss by searching materials with higher electrical conductivity is apparently impractical. Hence, the only option left to significantly reduce the metal loss and, thereby, the RC delay is to eliminate or suppress the skin effect.

Recently, artificial bilayered metaconductor (ABMC) was theoretically and experimentally verified to enable skin effect suppression [11]–[13]. However, an external magnetic field was needed to ensure the magnetization saturated along the coplanar wave guide (CPW). In this work, we present an integrated self-biased low loss conductor featured with skin effect suppression by exploiting the intrinsic and shape anisotropy of the magnetic layers. Up to 70% loss reduction has been achieved at ∼10 GHz without changing the propagation wavelength.

II. Experiments

Coplanar wave guides were fabricated on top of a low-loss Schott AF45 glass wafer with various structural parameters (listed in Table I). The processing details can be found in our previous work [13]. To accommodate the stress/strain, the glass wafer was coated by a thin bisbenzocyclobutene (BCB) polymer layer prior to the metal deposition. The multilayer conductor consists twelve periods of alternating 40 nm thick Py $(\mathrm{Ni_{80}Fe_{20}})$ and 650 nm thick Cu layers (see Fig. 1).

Magnetic hysteresis loop measurements were carried out on a Princeton AGM2900 test apparatus. The samples were fabricated from single Py film or $\mathrm{Cu/Ni_{80}Fe_{20}}$ mulilayer stack, and then patterned into a 2-mm-long, and 90-μm-wide stripe (see Fig. 2). The B-H loop measurements were performed parallel (the blue curve) and perpendicular (the red curve) to the stripe, i.e., the easy and hard axis, respectively. Both the single $\mathrm{Ni_{80}Fe_{20}}$ layer and the $\mathrm{Cu/Ni_{80}Fe_{20}}$ multilayer stack show clear easy- and hard- axis magnetic B-H loops. The coercivity of the $\mathrm{Cu/Ni_{80}Fe_{20}}$ multilayer stack is roughly $4 \sim 5$ times greater than the single $\mathrm{Ni_{80}Fe_{20}}$ film. This is caused by the tremendous stress/strain induced by the sputtered $\mathrm{Ni_{80}Fe_{20}}$ layer.

The frequency dependence of permeability of a single magnetic film (see Fig. 3) was extracted from a microstrip testing

Manuscript received March 01, 2012; revised May 04, 2012; accepted May 13, 2012. Date of current version October 19, 2012. Corresponding author: Y. Zhuang (e-mail: yan.zhuang@wright.edu).

Color versions of one or more of the figures in this paper are available online at http://ieeexplore.ieee.org.

Digital Object Identifier 10.1109/TMAG.2012.2200660

TABLE I
DESIGN PARAMETERS OF ABMC COPLANAR WAVEGUIDES (CPWS): LENGTH (L) AND WIDTH (W_1) OF SIGNAL LINE, SPACING (W_2) BETWEEN SIGNAL LINE

Sample	L (μm)	W_1 (μm)	W_2 (μm)
#1	2000.0	30	20
#2	2000.0	30	40
#3	2000.0	50	30
#4	2000.0	50	40
#5	2000.0	70	20
#6	2000.0	70	30
#7	2000.0	70	40
#8	2000.0	90	30
#9	2000.0	90	40

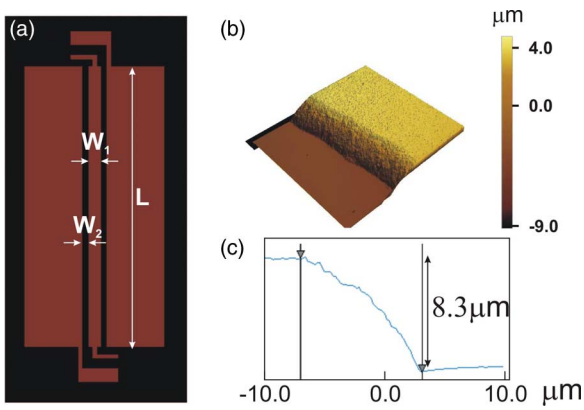

Fig. 1. (a) Sketch of coplanar wave guide,. (b) Surface morphology of a CPW measured by atomic force microscopy (AFM). (c) Line scan of CPW by AFM. The thickness of the ABMC layer is around 8.3 μm. Due to the wet chemical etching, the undercut is about 10 μm.

structure consisting of a 100-nm-thick $Ni_{80}Fe_{20}$ film, as described in the previous work [14]. The magnetic film was patterned into a rectangular prism with the length of 4 mm and width of 200 μm. The method was verified valid until 6 GHz. The accuracy gets worse at higher frequencies as both the real and imaginary parts of the permeability approach zero. For comparison, control devices built from copper were fabricated with the same configurations. The RF characterization was carried out on an Agilent PNA-L network analyzer. The pad parasitic was deembedded from the S-parameter by performing a separate set of measurement on a single "through" test fixture [15], [16].

III. RESULTS AND DISCUSSION

The AC resistance of the ABMC is governed by the effective skin depth $\delta_{\text{eff}} = (2/\omega\delta_{\text{eff}}\mu_{\text{eff}})^{1/2}$ where σ_{eff} and μ_{eff} are the effective conductivity and, permeability, respectively, of the ABMC

$$\sigma_{\text{eff}} = \frac{\sigma_{\text{NiFe}} t_{\text{NiFe}} + \sigma_{\text{Cu}} t_{\text{Cu}}}{t_{\text{NiFe}} + t_{\text{Cu}}} \quad (1)$$

$$\mu_{\text{eff}} = \mu_0 \frac{\mu_{\text{NiFe}} t_{\text{NiFe}} + t_{Cu}}{t_{\text{NiFe}} + t_{\text{Cu}}}. \quad (2)$$

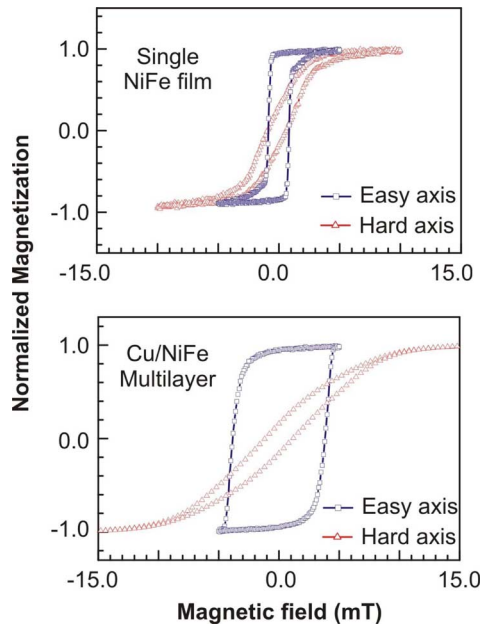

Fig. 2. Magnetic hysteresis loop measurements of a single 100 nm-thick $Ni_{80}Fe_{20}$ film and a $Cu(300\ nm)/Ni_{80}Fe_{20}(100\ nm)$ multilayer stack. Both of the samples were patterned into 2 mm long, and 90 μm wide stripes. The coercivity of the $Cu/Ni_{80}Fe_{20}$ multilayer is roughly 4 $\sim$ 5 times greater than the single $Ni_{80}Fe_{20}$ film. This is caused by the tremendous stress/strain induced by the sputtered $Ni_{80}Fe_{20}$ layer.

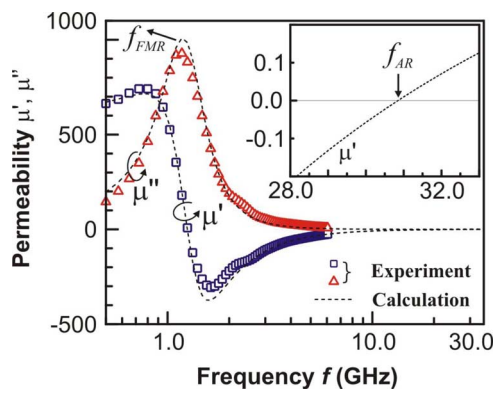

Fig. 3. Measured and simulated complex magnetic permeability versus frequencies of a single 100 nm thick $Ni_{80}Fe_{20}$ layer patterned with length—4 mm and width—200 μm. The real part of the permeability becomes negative beyond $\sim$1 GHz. The inset shows the enlarged plot of μ' in the vicinity of the anti-resonance frequency f_{AR}, onset of which μ' crosses zero. The dashed lines represent the calculated permeability by taking $\alpha = 2.5 \times 10^{-2}$.

Here $t_{\text{NiFe}}, t_{\text{Cu}}$ denote the thickness and $\sigma_{\text{NiFe}}, \sigma_{\text{Cu}}$ the conductivity of $Ni_{80}Fe_{20}$ and Cu layers, respectively. Moreover, μ_0 is the vacuum permeability, and μ_{NiFe} is the relative magnetic permeability of the ferromagnetic film magnetized in its plane and subject to an in-plane RF magnetic field applied normal to the magnetization [17]

$$\mu_{\text{NiFe}} = \frac{\omega_{\text{AR}}^2 - \omega^2}{\omega_{\text{FMR}}^2 - \omega^2} \quad (3)$$

$$\omega_{\text{AR}} = \gamma(M_s + H_0); \quad \omega_{\text{FMR}} = \gamma\sqrt{H_0(M_s + H_0)} \quad (4)$$

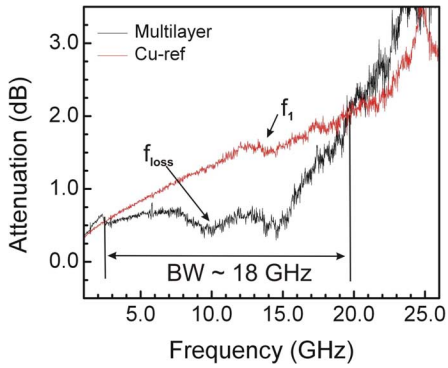

Fig. 4. Comparison of attenuation per centimeter versus frequency of a ABMC CPW (#1) and its copper counterpart. $f_{\rm loss}$ is the frequency when the attenuation constant (α) of the ABMC CPW reaches minimum. The decrease of α at frequency f_1 is not clear yet. Since this occurs to both ABMC and copper CPWs, it might be caused by the measurement system.

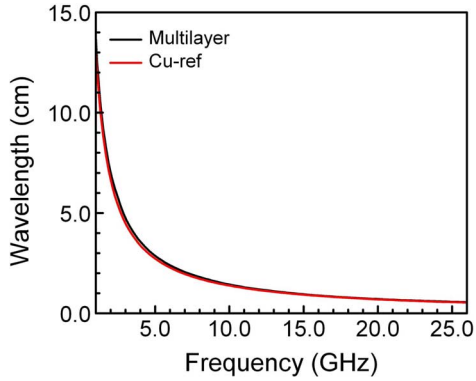

Fig. 5. Comparison of propagation wavelength versus frequency of a ABMC CPW (#1) and its copper counterpart.

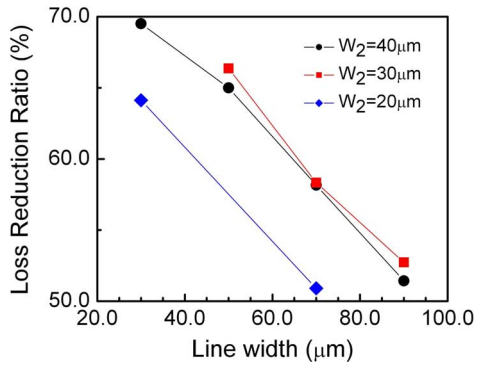

Fig. 6. Comparison of the loss reduction ratio (η) versus signal line width of ABMC CPWs (Table I), where $\eta = (\alpha_{\rm Copper} - \alpha_{\rm ABMC})/\alpha_{\rm Copper}$. $\alpha_{\rm Copper}$ and $\alpha_{\rm ABMC}$ are the attenuation constants of the copper and AMBC CPW, respectively.

where M_s is the saturation magnetization of the magnetic layers, H_0 is the shape-anisotropy field, and γ is the gyrotropic constant.

Near the ferromagnetic resonant frequency $\omega_{\rm FMR}$, the real part of the magnetic permeability approaches to zero. Beyond $\omega_{\rm FMR}$ this quantity exhibits a negative value (until one reaches the anti-resonant frequency $\omega_{\rm AR}$ where $\mu_{\rm NiFe} = 0$). At the frequency where $\mu_{\rm NiFe} = -t_{\rm Cu}/t_{\rm NiFe}$ (the effective anti-resonance frequency $\omega_{\rm EAR}$) the average permeability of the ABMC becomes nearly zero which results in a significant enhancement of the skin-depth [11] The frequency dependence of the loss of all the measured CPW lines can be fairly reproduced by using this model (equating the permeability to $-{\rm t_{Cu}/t_{NiFe}}$) as well as more elaborate calculations in [11], provided that an internal anisotropy field of ~500 Oe is used. This large field cannot be caused by shape effects as our calculations show, but might be due to the presence of very large stress/strain in the multilayer stack. Further research is, however, needed to investigate this phenomenon.

The measured attenuation per unit length and propagation wavelength versus frequencies of #1 and its copper counterpart are shown in Figs. 4 and 5, respectively. The propagation wavelength is only slightly different from each other. Unlike conventional conductors where the loss monotonically increases with frequency, the loss of ABMC CPW exhibited a broad dip between 2–20 GHz. Near the effective anti-resonance frequency (10 GHz), the average permeability of the ABMC becomes nearly zero leading to the aforementioned suppression of skin effect and the reduction of loss.

The second dip (at 15 GHz) observed in the loss of the ABMC lines in Fig. 4, cannot be explained by theoretical modeling. Model calculations as well as full wave electromagnetic simulations show a single broad dip. However, the dip near 15 GHz was observed on copper reference device as well, indicating a similar origin for the two devices. To further investigate the phenomenon measurements were performed on a large variety of devices with various geometrical parameters, listed in Table I. It turns out that for all ABMC and copper devices a loss dip occurred at ~15 GHz. Though the exact origin of this effect is not clear yet, it is very likely caused by the tip-to-pad and pad-to-device discontinuity [18], [19].

Fig. 6 compares the loss reduction ratio (η) versus signal line width of ABMC CPWs (see Table I) at $f_{\rm loss}$, where $f_{\rm loss}$ is indicated in Fig. 4. Up to 70% loss reduction has been achieved at ~10 GHz without changing the propagation wavelength. As the line width increases, the demagnetizing field perpendicular to the CPW line becomes weaker, resulting in distortion of magnetic alignment from its easy axis. Moreover, note that the etching process for patterning the ABMC films generates significant under etching [see Fig. 1(b) and (c)]. As a result, the actual width of the lines is less than the design value. Were it not for this effect the loss reduction of the ABMC-based CPWs could be further enhanced as simulations indicate.

The frequency range where skin-effect suppression is achieved is limited by the properties of the magnetic layers used. The maximum frequency where skin-effect suppression is observed coincides with the antiresonance frequency of a single magnetic layer. Table II lists examples of the saturation magnetization and anti-resonance frequencies of some common ferromagnetic materials.

It is worth mentioning that reducing the conductor loss will have a much less pronounced effect if the substrate loss dominates. Nonetheless, there are scenarios where ABMC may still be useful on normal Si substrates. Current IC process technology allows relatively thick insulating SiO_2 layers (~10 μm) to be placed in between Si and the metal. This will reduce substrate coupling and, therefore, substrate loss. In these circumstances using ABMC-based devices will still

TABLE II
ANTIRESONANCE FREQUENCY OF COMMON SOFT MAGNETIC MATERIALS [20]

Material	Saturation magnetization (Tesla)	Antiresonance frequency (GHz)
$Ni_{80}Fe_{20}$ (Permalloy)	1.1	30
$Ni_{50}Fe_{50}$ (Deltamax)	1.6	45
$Co_{50}Fe_{50}$ (Permendur)	2.4	67
FeCoB	1.9	53
Fe	2.2	61
3% SiFe	2.0	56

yield significant loss reduction. Finally, take notice that the mechanism of loss reduction in ABMC (skin-effect cancellation) is fundamentally different from that of the widely used conductor-insulator laminates which rely on eddy-current blockage by the insulating layers.

IV. CONCLUSION

We have demonstrated that, by properly tailoring the thickness ratio, the ABMC conductor shows a significant reduction of the ohmic loss at radio frequencies due to a suppression of the skin-effect. Up to 70% loss reduction has been achieved by meta-conductor based coplanar wave guide at $\sim$ 10 GHz without changing the propagation wavelength.

ACKNOWLEDGMENT

The authors would like to thank Prof. J. N. Burghartz from Institute for Microelectronics Stuttgart, Germany, and Dr. M. Vroubel from NXP for many useful discussions.

REFERENCES

[1] M. Morgen *et al.*, "Low dielectric constant materials for ULSI interconnects," *Annu. Rev. Mater. Sci.*, vol. 30, pp. 645–680, 2000.
[2] R. Rosenberg *et al.*, "Copper metallization for high performance silicon technology," *Annu. Rev. Mater. Sci.*, vol. 30, pp. 229–262, 2000.
[3] R. H. Havemann and J. A. Hutchby, "High-performance interconnects: An integration overview," *Proc. IEEE*, vol. 89, no. 5, pp. 586–601, May 2001.
[4] P. J. Restle *et al.*, "A clock distribution network for microprocessors," *IEEE J. Solid-State Circuits*, vol. 36, no. 5, pp. 792–799, May 2001.
[5] J. D. Meindl *et al.*, "Limits on silicon nanoelectronics for terascale integration," *Science*, vol. 293, pp. 2044–2048, 2001.
[6] A. V. Mule *et al.*, "Electrical and optical clock distribution networks for gigascale microprocessors," *IEEE Trans. VLSI Syst.*, vol. 10, no. 5, pp. 582–594, Oct. 2002.
[7] Y. Elboim *et al.*, "A clock-tuning circuit for system-on-chip," *IEEE Trans. VLSI Syst.*, vol. 11, no. 4, pp. 616–626, Aug. 2003.
[8] J. D. Meindl, "Interconnect opportunities for gigascale integration," *IEEE MICRO*, vol. 23, no. 3, pp. 28–35, May-Jun. 2003.
[9] S. C. Chan *et al.*, "Uniform-phase uniform-amplitude resonant-load global clock distributions," *IEEE J. Solid-State Circuits*, vol. 40, no. 1, pp. 102–109, Jan. 2005.
[10] "2005 International Technology Roadmap for Semiconductors" [Online]. Available: http://public.itrs.net
[11] B. Rejaei and M. Vroubel, "Suppression of skin-effect in metal/ferromagnet superlattice conductors," *J. Appl. Phys.*, vol. 96, pp. 6863–6868, 2004.
[12] Y. Zhuang, B. Rejaei, H. Schellevis, M. Vroubel, and J. N. Burghartz, "Magnetic-multilayered interconnects featuring skin effect suppression," *IEEE Electron Device Lett.*, vol. 29, no. 4, pp. 319–321, Apr. 2008.
[13] I. Iramnaaz, T. Sandoval, Y. Zhuang, H. Schellevis, and B. Rejaei, "High quality factor RF inductors using low loss conductor featured with skin effect suppression for standard CMOS/BiCMOS," in *Proc. IEEE 61st ECTC*, Lake Buena Vista, FL, May 2011, pp. 163–168.
[14] M. Vroubel, Y. Zhuang, B. Rejaei, and J. N. Burghartz, "Investigation of microstrips with NiFe magnetic thin film (II): Modelling," *Trans. Magn. Soc. Japan*, vol. 2, pp. 371–376, 2002.
[15] Y. Tretiakov, K. Vaed, D. Ahlgren, J. Rascoe, S. Venkatadri, and W. Woods, "On wafer de-embedding for SiGe/BiCMOS/RFCMOS transmission line interconnect characterization," in *Proc. Interconnect Tech. Conf.*, Burlingame, CA, Jun. 2004, pp. 166–168.
[16] E. S. Daniel, N. E. Harff, V. Sokolov, S. M. Schreiber, and B. K. Gilbert, "Network analyzer measurement de-embedding utilizing a distributed transmission matrix bisection of a single THRU structure," in *Proc. ARFTG Conf. Digest Spring*, Ft Worth, TX, Jun. 2004, pp. 61–68.
[17] A. G. Gurevich and G. A. Melkov, *Magnetization Oscillations and Waves*. New York: CRC, 1996.
[18] J. Lim, D. Kwon, J.-S. Rieh, S.-W. Kim, and S. W. Hwang, "RF characterization and modeling of various wire bond transitions," *IEEE Trans. Adv. Packag.*, vol. 28, no. 4, pp. 772–778, Nov. 2005.
[19] D. F. Williams, "On-wafer measurement at millimeter wave frequencies," in *IEEE MTT-S Int. Microw. Symp. Dig.*, San Francisco, CA, Jun. 1996, vol. 3, pp. 1683–1686.
[20] O'Handley, *Modern Magnetic Materials*. New York: Wiley, 2000.